Toward Functional Models of the Nickel Sites in [FeNi] and [FeNiSe] Hydrogenases: Syntheses, Structures, and Reactivities of Nickel(II) Complexes Containing $[NiN_3S_2]$ and $[NiN_3Se_2]$ Chromophores

Christine A. Marganian,[†] Haresh Vazir,[†] Narayan Baidya,[†] Marilyn M. Olmstead,[‡] and Pradip K. Mascharak*,[†,§]

Contribution from the Department of Chemistry and Biochemistry, University of California, Santa Cruz, California 95064, and Department of Chemistry, University of California, Davis, California 95616

Received April 18, 1994[⊗]

Abstract: The reaction of $[Ni(terpy)Cl_2]$ with ~2 equiv of $2,4,6\text{-}(Me)_3C_6H_2Se^-$ in 3:1 acetonitrile/ethanol affords $[Ni(terpy)(2,4,6\text{-}(Me)_3C_6H_2Se)_2]$ (**7**), while $[Ni(DAPA)Cl_2]$ (DAPA = 2,6-bis[1-(phenylimino)ethyl]pyridine) reacts with ~2 equiv of PhS^- and $PhSe^-$ in neat ethanol or acetonitrile to yield $[Ni(DAPA)(SPh)_2]$ (**8**) and $[Ni(DAPA)(SePh)_2]$ (**9**), respectively. All three complexes contain the distorted trigonal bipyramidal (TBP) NiN_3E_2 (E = S, Se) chromophore. Previous X-ray absorption spectroscopic data have indicated a distorted TBP NiN_3S_2 coordination for the nickel site of the hydrogenase (H_2ase) from *Thiocapsa roseopersicina*. Complex **7** crystallizes in the monoclinic space group $P2_1/n$ with $a = 13.170(6)$ Å, $b = 16.091(5)$ Å, $c = 15.111(8)$ Å, $\beta = 114.42(2)°$, $V = 2916(2)$ Å^3, and $Z = 4$. The structure of **7** was refined to $R = 4.78\%$ on the basis of 2730 reflections ($I > 4\sigma(I)$). Complex **8**·CH_3CN crystallizes in the monoclinic space group $P2_1/c$ with $a = 23.012(7)$ Å, $b = 17.814(5)$ Å, $c = 15.698(4)$ Å, $\beta = 108.52(2)°$, $V = 6099(5)$ Å^3, and $Z = 8$. The structure of **8**·CH_3CN was refined to $R = 6.46\%$ on the basis of 6133 reflections ($I > 4\sigma(I)$). Complex **9**·CH_3CN also crystallizes in the monoclinic space group $P2_1/c$ with $a = 23.209(2)$ Å, $b = 17.960(1)$ Å, $c = 15.749(1)$ Å, $\beta = 108.482(6)°$, $V = 6225$ Å^3, and $Z = 8$. The structure of **9**·CH_3CN was refined to 3.90% on the basis of 5808 reflections ($I > 4\sigma(I)$). Reduction of the terpy analogue **7** with aqueous dithionite gives rise to the corresponding Ni(I) complex which binds CO (reversibly) and H^-. The EPR parameters of the CO and hydride adducts resemble the Ni-CO and Ni-C signal of the H_2ases. Much like the other terpy analogues reported previously by this group, oxidation of **7** affords unstable Ni(III) products in low yields. The two DAPA analogues (**8** and **9**), on the other hand, are readily oxidized and reduced by biologically relevant oxidants and reductants, and the transformation Ni(III) ← Ni(II) → Ni(I) is reversible. The Ni(III) species (**10** and **13**) derived from **8** and **9** via oxidation with $[Fe(CN)_6]^{3-}$ are comparatively stable and do not bind CO (or H^-). The single electron in both **10** and **13** resides in the d_{z^2} orbital. Upon reduction with aqueous dithionite, **8** and **9** produce the corresponding Ni(I) species **11** and **14** with the single electron in the $d_{x^2-y^2}$ orbital. These Ni(I) complexes are quite stable at low temperatures but slowly lose thiolates/selenolates at room temperature to give $[Ni(DAPA)(solv)_2]^+$. Both **11** and **14** bind CO reversibly. The affinity of the Ni(I) (but not the Ni(III)) model complexes toward CO strongly suggests the presence of Ni(I) in the C form of the H_2ases since the enzymes bind CO only in the Ni-C form. Reaction of $NaBH_4$ with **8** and **9** results in the hydride adducts **19** and **20**. These hydride adducts are stable under basic conditions. The absence of any detectable proton hyperfine coupling indicates that the H^- ligand is located at the basal plane of the Ni(I) center. The EPR parameters of the CO and hydride adducts are quite similar to those of the Ni-CO and Ni-C signals of the H_2ases. Under basic conditions, both **8** and **9** react with dihydrogen at ambient temperature and pressure to afford the hydride adducts **19** and **20** in significant yields. This reaction is quite remarkable since the model complexes mimic the reductive activation step of the biological nickel site in such a reaction to ultimately produce Ni-C-like signals. Taken together, the present results strongly suggest a Ni(I)−H^- formalism for the nickel site in the C form of the H_2ases. In addition, enhancement of the intensities of the EPR signals of the hydride adducts in the presence of a base indicates heterolytic cleavage of H_2 (coordinated or not) at the Ni(I) site of the model complexes and probably also at the enzyme active sites.

Introduction

Hydrogenases (H_2ases) are metalloenzymes that catalyze the reversible oxidation of dihydrogen ($H_2 \rightleftharpoons 2H^+ + 2e$) and are involved in the production and consumption of H_2 by various microorganisms.[1-5] Depending on their metal contents, H_2ases have been grouped into three classes, namely, (i) Fe hydrogenases, containing Fe−S clusters, (ii) [FeNi] hydrogenases, containing Fe−S clusters and 1 equiv of Ni, and (iii) [FeNiSe] hydrogenases, containing Fe−S clusters and 1 equiv of Ni with one ligated Se donor atom.[1] Spectroscopic studies on the Ni-containing H_2ases implicate the Ni center as the enzyme active site where binding of substrate and inhibitor molecules occurs.[6] Most of the Ni-containing H_2ases exhibit characteristic EPR spectra at relatively higher temperatures (liquid N_2) that are associated with the different redox states of the nickel site(s).[1-3] In the "as-isolated" form, [FeNi] H_2ases display rhombic EPR signals (denoted as Ni-A, $g = 2.31, 2.23, 2.02$, and Ni-B, $g = 2.33, 2.16, 2.02$). Incubation of the enzymes under dihydrogen

[†] University of California, Santa Cruz.
[‡] University of California, Davis.
[§] Alfred P. Sloan Research Fellow, 1993−1995.
[⊗] Abstract published in *Advance ACS Abstracts*, December 1, 1994.

0002-7863/95/1517-1584$09.00/0

(reduction) leads to disappearance of these signals. Upon further reduction, the enzymes exhibit another rhombic signal (Ni-C, g = 2.19, 2.14, 2.02) that correlates with the hydrogenase activity. These EPR signals are believed to be associated with the "unready" (Ni-A), "ready" (Ni-B), and the "catalytically active" state (Ni-C) of the enzyme. Since nickel is EPR-active in both +3 (d^7) and +1 (d^9) oxidation states, assignment of the redox states of the biological nickel center in these different forms of the enzyme is not quite straightforward. So far, two distinctly different mechanisms have been proposed on the basis of physicochemical data. One of these working hypotheses assumes the existence of Ni(III) throughout the entire catalytic cycle,[1c,f,7] while the other involves nickel as a redox-active metal and assigns Ni(III) (Ni-A, Ni-B), Ni(II) (EPR-silent), and Ni(I) (Ni-C) at the active site during the processes of H_2 consumption/evolution.[1e,2a,b,6,8] Reversible binding of CO (an inhibitor) to the reduced form of the enzyme[6] and the photodissociative nature of the Ni-C species[6] support the existence of Ni(I) in the latter mechanism.

Recent X-ray absorption spectroscopic (XAS) data on the [FeNi] H_2ase from the purple photosynthetic bacterium *Thiocapsa roseopersicina* indicate that the active site nickel most probably exists in a trigonal bipyramidal (TBP) geometry and is ligated to 3−4 N/O and ~2 S donor atoms at 2.06 and 2.21 Å, respectively.[9] Along this line, we have reported several designed model complexes containing the [NiN_3S_2] chromophore in TBP geometry that are good *structural* models for the biological nickel site.[10] In the first group of model complexes (analogues), the tridentate aromatic ligand terpy (terpy = 2,2′,2″-terpyridine) provided the three N donor atoms around the nickel center, while the two S donor atoms belonged to aromatic thiolates with bulky substituents on the phenyl rings.[10] Controlled ligand basicities and proper steric crowding in the first coordination sphere of the metal center allowed the successful isolation of the desired mononuclear pentacoordinated Ni(II) complexes in these attempts. In addition, this strategy provided an open sixth site where small molecules like CO could bind. All three complexes with the terpy ligand, namely, [Ni(terpy)(C_6F_5S)$_2$] (**1**), [Ni(terpy)(2,4,6-(i-Pr)$_3C_6H_2S$)$_2$] (**2**), and [Ni(terpy)(2,6-$(Me)_2C_6H_3S$)$_2$] (**3**), are readily reduced to the Ni(I) species which bind CO reversibly. These complexes are also capable of binding H^- at low temperatures. The fact that the EPR parameters of the hydride adducts [Ni(terpy)$(RS)_2(H^-)]^{2-}$ are comparable to those of the Ni-C signal of the enzyme prompted us to suggest a Ni(I)−H^- formalism for the Ni-C intermediate. Despite these similarities between the reduced model complexes and the C form of the enzyme, the terpy complexes do not qualify as good functional models since oxidation of the complexes to the corresponding Ni(III) species is insubstantial even at low temperatures.

The XAS studies have also indicated that the coordination structure of the nickel site in the [FeNiSe] H_2ase from *Desulfovibrio baculatus*[11a] is very similar to that in the *T. roseopersicina* H_2ase. The nickel in the *D. baculatus* active site is ligated to 3−4 N/O atoms at 2.06 Å, 1−2 S/Cl atoms at 2.1 Å, and 1 Se atom at 2.44 Å. Both the results of the Se XAS studies and the identification of a selenocysteine codon (TGA) in the large subunit gene of the [FeNiSe] H_2ase from *D. baculatus*[12] strongly suggest the presence of a selenocysteine residue coordinated to the nickel center. Magnetic susceptibility studies on the EPR-silent state of the enzyme indicate a diamagnetic species, which is consistent with a Ni(II) center in a five-coordinated environment.[13] However, the reactivities and the catalytic properties of the S- and Se-containing enzymes are quite different.[7a,11] In order to investigate the unique role of Se ligation to Ni in the [FeNiSe] H_2ases, we have recently synthesized and structurally characterized analogues of the compositions [Ni(terpy)$(PhSe)_2]_2$ (**4**), [Ni(dmp)(2,4,6-$(Me)_3C_6H_2$-$Se)_2$], (**5**) [Ni(dmp)$(PhSe)_2]_2$·$2CH_3CN$ (**6**) (dmp = 2,9-dimethyl-1,10-phenanthroline), and [Ni(terpy)(2,4,6-$(Me)_3C_6H_2Se)_2$] (**7**) that contain NiN_xSe_y chromophores in various geometries.[14] Out of this group of analogues, only [Ni(terpy)(2,4,6-$(Me)_3C_6H_2$-$Se)_2$] (**7**) exhibits the desired distorted TBP geometry with an average Ni−Se bond distance of 2.43 Å, a value close to that predicted for the Ni site in the *D. baculatus* H_2ase. Preliminary experiments[14] have shown that the reduced Ni(I) species derived from **7** and its CO adduct give rise to EPR signals similar to its thiolate analogue [Ni(terpy)(2,6-$(Me)_2C_6H_3S$)$_2$] (**3**).[10a] However, much like the thiolate analogue, oxidation of **7** to the cor-

(1) (a) Przybla, A. E.; Robbins, J.; Menon, N.; Peck, H. D., Jr. *FEMS Microbiol. Rev.* **1992**, *88*, 109. (b) Moura, J. J. G.; Moura, I.; Teixeira, M.; Xavier, A. V.; Fauque, G. D.; LeGall, J. *Met. Ions Biol. Syst.* **1988**, *23*, 285. (c) Moura, J. J. G.; Teixeira, M.; Moura, I.; LeGall, J. In *The Bioinorganic Chemistry of Nickel*; Lancaster, J. R., Jr., Ed.; VCH Publishers: Deerfield Beach, FL, 1988; Chapter 9, p 191. (d) Bastian, N. R.; Wink, D. A.; Wackett, L. P.; Livingston, D. J.; Jordan, L. M.; Fox, J.; Orme-Johnson, W. H.; Walsh, C. T. In *The Bioinorganic Chemistry of Nickel*; Lancaster, J. R., Jr.; Ed.; VCH Publishers: Deerfield Beach, FL, 1988; Chapter 10, p 227. (e) Cammack, R.; Fernandez, V. M.; Schneider, K. In *The Bioinorganic Chemistry of Nickel*; Lancaster, J. R., Jr., Ed.; VCH Publishers: Deerfield Beach, FL, 1988; Chapter 8, p 167. (f) Moura, J. J. G.; Teixeira, M.; Moura, I.; Xavier, A. V.; LeGall, J. In *Frontiers in Bioinorganic Chemistry*; Xavier, A. V., Ed.; VCH Publishers: Deerfield Beach, FL, 1986; p 3.

(2) (a) Cammack, R. *Adv. Inorg. Chem.* **1988**, *32*, 297. (b) Albracht, S. P. J.; van der Zwaan, J. W.; Fontijn, R. D.; Slater, E. C. In *Frontiers in Bioinorganic Chemistry*; Xavier, A. V., Ed.; VCH Publishers: Deerfield Beach, FL, 1986; p 11. (c) Cammack, R.; Hall, D. O.; Rao, K. K. In *Gas Metabolism: Mechanistic, Metabolic and Biotechnological Aspects*; Poole, R. K., Dow, C. S., Eds.; Academic Press: New York, 1985.

(3) (a) Hausinger, R. P. *Microbiol. Rev.* **1987**, *51*, 22. (b) Walsh, T. C.; Orme-Johnson, W. H. *Biochemistry* **1987**, *26*, 4901.

(4) (a) Fauque, G.; Peck, H. D., Jr.; Moura, J. J. G.; Huynh, B. H.; Berlier, Y.; DerVartanian, D. V.; Teixeira, M.; Przybyla, A. E.; Lespinat, P. A.; Moura, I.; LeGall, J. *FEMS Microbiol. Rev.* **1988**, *54*, 299. (b) Vignais, P. M.; Colbeau, A.; Willison, J. C.; Jouranneau, Y. *Adv. Microb. Physiol.* **1985**, *26*, 155.

(5) (a) Moura, J. J. G.; Teixeira, M.; Moura, I. *J. Mol. Catal.* **1984**, *23*, 303. (b) Kondratieva, E. N.; Gogotov, I. N. *Adv. Biochem. Eng./Biotechnol.* **1983**, *28*, 139. (c) Adams, M. M. W.; Mortenson, L. E.; Chen, J. S. *Biochim. Biophys. Acta* **1980**, *594*, 105.

(6) (a) van der Zwaan, J. W.; Coremans, J. M. C. C.; Bouwens, E. C. M.; Albracht, S. P. J. *Biochim. Biophys. Acta* **1990**, *1041*, 101. (b) Coremans, J. M. C. C.; van der Zwaan, J. W.; Albracht, S. P. J. *Biochim. Biophys. Acta* **1989**, *997*, 256. (c) van der Zwaan, J. W.; Albracht, S. P. J.; Fontijn, R. D.; Roelofs, Y. B. M. *Biochim. Biophys. Acta* **1986**, *872*, 208. (d) van der Zwaan, J. W.; Albracht, S. P. J.; Fontijn, R. D.; Slater, E. C. *FEBS Lett.* **1985**, *179*, 271.

(7) (a) Moura, J. J. G.; Teixeira, M.; Moura, I. *Pure Appl. Chem.* **1989**, *61*, 915. (b) Teixeira, M.; Moura, I.; Xavier, A. V.; Huynh, B. H.; DerVartanian, D. V.; Peck, H. D., Jr.; LeGall, J.; Moura, J. J. G. *J. Biol. Chem.* **1985**, *260*, 8942.

(8) Cammack, R.; Fernandez, V. M.; Schneider, K. *Biochimie* **1986**, *68*, 85. (b) Fernandez, V. M.; Hatchikian, E. C.; Patil, D. S.; Cammack, R. *Biochim. Biophys. Acta* **1986**, *883*, 145.

(9) (a) Bagyinka, C.; Whitehead, J. P.; Maroney, M. J. *J. Am. Chem. Soc.* **1993**, *115*, 3576. (b) Maroney, M. J.; Colpas, G. J.; Bagyinka, C.; Baidya, N.; Mascharak, P. K. *J. Am. Chem. Soc.* **1991**, *113*, 3962. (c) Colpas, G. J.; Maroney, M. J.; Bagyinka, C.; Kumar, M.; Willis, W. S.; Suib, S. L.; Baidya, N.; Mascharak, P. K. *Inorg. Chem.* **1991**, *30*, 920.

(10) (a) Baidya, N.; Olmstead, M. M.; Whitehead, J. P.; Bagyinka, C.; Maroney, M. J.; Mascharak, P. K. *Inorg. Chem.* **1992**, *31*, 3612. (b) Baidya, N.; Olmstead, M. M.; Mascharak, P. K. *Inorg. Chem.* **1991**, *30*, 929.

(11) (a) Eidsness, M. K.; Scott, R. A.; Prickril, B. C.; DerVartanian, D. V.; LeGall, J.; Moura, I.; Moura, J. J. G.; Peck, H. D., Jr. *Proc. Natl. Acad. Sci. U.S.A.* **1989**, *86*, 147. (b) He, S. H.; Teixeira, M.; LeGall, J.; Patil, D. S.; Moura, I.; Moura, J. J. G.; DerVartanian, D. V.; Huynh, B. H.; Peck, H. D., Jr. *J. Biol. Chem.* **1989**, *264*, 2678. (c) Teixeira, M.; Fauque, G.; Moura, I.; Lespinat, P. A.; Berlier, Y.; Prickril, B.; Peck, H. D., Jr.; Xavier, A. V.; LeGall, J.; Moura, J. J. G. *Eur. J. Biochem.* **1987**, *167*, 47. (d) Teixeira, M.; Moura, I.; Fauque, G.; Czechowski, M.; Berlier, Y.; Lespinat, P. A.; LeGall, J.; Xavier, A. V.; Moura, J. J. G. *Biochimie* **1986**, *68*, 75.

(12) Voordouw, G.; Menon, N. K.; LeGall, J.; Choi, E.; Peck, H. D., Jr.; Przybyla, A. E. *J. Bacteriol.* **1989**, *171*, 2894.

(13) Wang, C.-P.; Franco, R.; Moura, J. J. G.; Moura, I.; Day, E. P. *J. Biol. Chem.* **1992**, *267*, 7378.

(14) Baidya, N.; Noll, B. C.; Olmstead, M. M.; Mascharak, P. K. *Inorg. Chem.* **1992**, *31*, 2999.

responding Ni(III) species does not proceed to a great extent at subzero temperatures.

Since our goal is to design a model system containing the $[NiN_3E_2]$ (E = S, Se) chromophore that readily affords the Ni(III) and Ni(I) species with biologically relevant oxidants and reductants (including H_2), we replaced terpy with 2,6-bis[1-(phenylimino)ethyl]pyridine (DAPA) as the 3N donor ligand. DAPA contains "harder" N donor atoms and a less extensive π system. The nickel complexes of this tailored ligand demonstrate superior complex stability upon both oxidation and reduction of the Ni(II) center. In a previous communication,[15] we reported the synthesis and structure of [Ni(DAPA)(SPh)$_2$] (**8**) and its redox properties. **8** is the first structural model of the [FeNi] H_2ases that produces the oxidized (Ni(III)) and the reduced (Ni(I)) NiN_3S_2 chromophore in a reversible manner. We have now isolated and structurally characterized [Ni(DAPA)(SePh)$_2$] (**9**). Both these DAPA complexes bind H^- more readily than the terpy analogues and can be reduced by H_2 to produce the hydride adducts $[Ni^I(DAPA)(PhE)_2(H^-)]^{2-}$ (E = S, Se). In this paper, we report the syntheses and structural features of **7**–**9** in detail. Also reported are the results of the EPR studies on the (a) Ni(III) and Ni(I) complexes derived chemically from **7**–**9**, (b) binding of CO by these Ni(III) and Ni(I) species, and (c) reaction of H_2 and H^- with the Ni(II) and Ni(I) complexes. Complexes **7**–**9** are the first examples of model Ni(II) complexes that react with H_2 at ambient temperature and pressure to afford Ni(I)–H^- species. Results from section c provide compelling evidence in favor of a Ni(I)–H^- formalism for the active intermediate associated with the Ni-C signal. Heterolytic cleavage of an H–H bond at the Ni(I) site has also been proposed on the basis of these data.

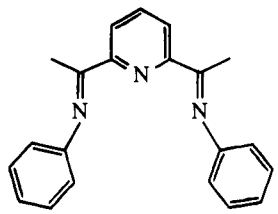

DAPA

Experimental Section

Thiophenol and selenophenol were purchased from Aldrich Chemical Co. and were used without further purification. Bis(2,4,6-trimethylphenyl) diselenide was purchased from Lancaster and used as received. [Ni(terpy)Cl$_2$] and [Ni(DAPA)Cl$_2$] were synthesized from modified published procedures.[16] In the following syntheses, degassed solvents were used, and all manipulations were performed under an atmosphere of pure and dry dinitrogen.

[Ni(terpy)(2,4,6-(Me)$_3$C$_6$H$_2$Se)$_2$] (7). A solution of Na(2,4,6-(Me)$_3$C$_6$H$_2$Se), prepared from 200 mg (0.51 mmol) of bis(2,4,6-trimethylphenyl) diselenide and 37.9 mg (1.0 mmol) $NaBH_4$ in 5 mL of ethanol, was slowly added with stirring to a suspension of 165 mg (0.45 mmol) of [Ni(terpy)Cl$_2$] in 15 mL of acetonitrile. The resulting dark purple solution was stirred for 2 h, whereupon shiny dark purple microcrystalline material separated. The compound was collected by filtration and dried under vacuum. The product was recrystallized from warm acetonitrile. Crystals for the X-ray work were obtained from slow cooling of the mother liquor. The combined yield was 260 mg (84%). Anal. Calcd for $C_{33}H_{33}N_3Se_2Ni$: C, 57.59; H, 4.83; N, 6.10. Found: C, 57.54; H, 4.76; N, 6.06. Selected IR bands (KBr pellet, cm^{-1}): 2908 (m), 1596 (m), 1561 (m), 1449 (s), 1020 (m), 850 (m), 773 (s), 709 (w). Value of μ_{eff}(298 K, polycrystalline): 3.32 μ_B.

[Ni(DAPA)(SPh)$_2$] (8). A solution of 230 mg (1.0 mmol) of Et_4NSPh in 15 mL of ethanol was slowly added with stirring to 195 mg (0.45 mmol) of [Ni(DAPA)Cl$_2$] in 20 mL of ethanol. The resulting dark reddish brown solution was stirred for 1 h, whereupon shiny dark brown microcrystalline material separated. The compound was collected by filtration, washed with ethanol, and dried under dinitrogen. The yield was 230 mg (90%). Anal. Calcd for $C_{35}H_{35}N_3OS_2Ni$ (**8**·C_2H_5OH): C, 66.04; H, 5.53; N, 6.63. Found: C, 65.50; H, 5.34; N, 6.67. Selected IR bands (KBr pellet, cm^{-1}): 3050 (m), 2965 (w), 2895 (w), 1577 (vs), 1485 (s), 1430 (m), 1261 (s), 1228 (s), 1080 (s), 1025 (m), 810 (w), 780 (s), 732 (vs), 715 (s), 696 (vs), 480 (m). Value of μ_{eff} (298 K, polycrystalline): 2.89 μ_B.

[Ni(DAPA)(SPh)$_2$]·CH$_3$CN (8·CH$_3$CN) was synthesized in acetonitrile. Crystals for the X-ray work were obtained from slow cooling of the mother liquor.

[Ni(DAPA)(SePh)$_2$] (9). A solution of Me_4NSePh, prepared from 91 mg (0.5 mmol) of $Me_4NOH·5H_2O$ and 50 μL (0.5 mmol) of benzeneselenol in 7 mL of ethanol was slowly added with stirring to 100 mg (0.23 mmol) of [Ni(DAPA)Cl$_2$] in 7 mL of ethanol. The color of the reaction mixture turned dark brown. After stirring for 1 h, the dark brown shiny microcrystalline product was collected by filtration, washed with ethanol, and dried under dinitrogen (yield = 120 mg, 76%). Anal. Calcd for $C_{35}H_{35}N_3OSe_2Ni$ (**9**·C_2H_5OH): C, 57.56; H, 4.83; N, 5.75. Found: C, 57.54; H, 4.82; N, 5.75. Selected IR bands (KBr pellet, cm^{-1}): 3050 (w), 2960 (w), 1572 (s), 1485 (s), 1430 (m), 1263 (s), 1227 (m), 1068 (m), 1020 (m), 808 (m), 778 (s), 730 (vs), 699 (s). Value of μ_{eff} (298 K, polycrystalline): 3.15 μ_B.

[Ni(DAPA)(SePh)$_2$]·CH$_3$CN (9·CH$_3$CN) was synthesized in acetonitrile. Slow cooling of the mother liquor afforded crystals suitable for crystallographic measurements.

X-ray Data Collection, Structure Solution, and Refinement. Diffraction experiments were performed at 130 K on either a Siemens P4 machine or a Syntex P2$_1$ machine. Both machines were equipped with a modified LT-1 low-temperature apparatus. Nickel-filtered Cu Kα radiation (λ = 1.541 78 Å) from a Siemens rotating anode source was employed for **7** and **9**·CH$_3$CN, while for **8**·CH$_3$CN Mo Kα radiation (λ = 0.710 69 Å) was used. Only random fluctuations of <1% in the intensities of two standard reflections were observed during the course of data collection. The structures were solved by direct methods.[17,18] For all three complexes, the space groups were uniquely determined by the observation of systematic absences. Hydrogen atoms bonded to the carbon atoms were included at calculated positions with C–H of 0.96 Å (0.99 Å for methyl H) and were refined by using a riding model and an isotropic U of 0.035 Å^2. The data were corrected for absorption effects by use of the program XABS.[19]

The structure of **7** was refined by the full-matrix least-squares method, while for **8**·CH$_3$CN and **9**·CH$_3$CN the block-diagonal least-squares method was used. One of the Se atoms of **7** is disordered. Initially, the two atoms of the disordered pair were refined with variable occupancy. Since the refined occupancies were 0.506 and 0.494, they were fixed at 0.50 for both atoms in subsequent cycles of refinement. The disordered Se(1) atoms were refined isotropically, and the average position is shown in Figure 1. Except for this case, anisotropic thermal parameters were assigned to all non-hydrogen atoms of **7**–**9** in the final cycles of refinement. The final difference maps were practically featureless. Machine parameters, crystal data, and data collection parameters are summarized in Table 1. Selected bond distances and angles are listed in Table 2. The following data for **7**–**9** have been submitted as supplementary material: atomic coordinates and isotropic thermal parameters for the non-hydrogen atoms (Tables S1–S3), complete lists of bond distances (Tables S4–S6) and angles (Tables S7–S9), anisotropic thermal parameters (Tables S10–S12), H atom coordinates (Tables S13–S15), and values of 10$|F_o|$ and 10$|F_c|$ (Tables S16–S18).

(15) Baidya, N.; Olmstead, M. M.; Mascharak, P. K. *J. Am. Chem. Soc.* **1992**, *114*, 9666.

(16) (a) Judge, J. S.; Reiff, W. M.; Intille, G. M.; Ballway, P.; Baker, W. A. *J. Inorg. Nucl. Chem.* **1967**, *29*, 1711. (b) Alyea, E. C.; Ferguson, G.; Restivo, R. J. *Inorg. Chem.* **1975**, *14*, 2491.

(17) Siemens SHELXTL PLUS (VMS) version 4.2 installed on a MicroVAX 3200 computer.

(18) Neutral-atom scattering factors were taken from the following: *International Tables for Crystallography*; D. Reidel Publishing Co.: Boston, 1991; Vol. C.

(19) Moezzi, B. Ph.D. Dissertation, University of California, Davis, 1987. The program obtains an absorption tensor from $F_o - F_c$ differences.

(20) (a) Cortes, R.; Arriortua, M. I.; Rojo, T.; Solans, X.; Miravitlles, C.; Beltran, D. *Acta Crystallogr., Sect. C: Cryst. Struct. Commun.* **1985**, *C41*, 1733. (b) Arriortua, M. I.; Rojo, T.; Amigo, J. M.; Germain, G.; Declerq, J. P. *Bull. Soc. Chim. Belg.* **1982**, *91*, 337.

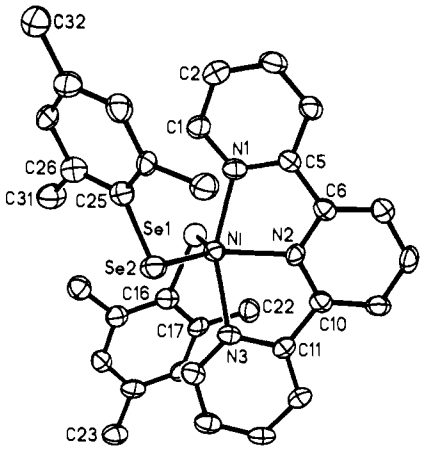

Figure 1. Thermal ellipsoid plot (50% probability level) of **7** with the atom-labeling scheme. The average position of the disordered Se(1) is shown. Hydrogen atoms are omitted for clarity.

Other Physical Measurements. Infrared spectra were obtained with a Perkin-Elmer 1600 spectrophotometer. A Nicolet 800 FTIR spectrophotometer was used to acquire the IR spectra of the CO adducts of the Ni(I) species (generated in DMF solutions). The solution cell was equipped with CaF_2 windows. Absorption spectra were recorded on a Perkin-Elmer Lambda-9 spectrophotometer. ^1H NMR spectra were measured on a General Electric 300-MHz GN-300 instrument. A Bruker ESP-300 spectrometer was used to record the EPR spectra at X-band frequencies. A Johnson Matthey magnetic susceptibility balance was used to measure the room temperature susceptibility values in the polycrystalline state.

Redox Reactions and Binding Studies. $(Et_4N)_3[Fe(CN)_6]$ was used as the oxidant, while $Na_2S_2O_4$, $NaBH_4$, and H_2 were employed as reductants. $NaBH_4$ and H_2 also served as H^- donors. For EPR studies, DMF solutions were placed in quartz EPR tubes, and the reactions were performed in the temperature range 233−298 K. The reaction mixtures were frozen immediately for EPR measurements, and the spectra were recorded at 100 K. Typically, 0.3 mL of a 10 mM solution of the compound in DMF was mixed with 1.0 equiv of $(Et_4N)_3[Fe(CN)_6]$ in 20 μL of 1:1 DMF/methanol at 233 K to generate the oxidized species. The reduced species was obtained by the addition of 0.5 equiv of $Na_2S_2O_4$ in 10 μL of H_2O at 298 K. The carbon monoxide adducts of the reduced species were produced by passing CO through solutions of the reduced complexes. The hydride adducts of the reduced species were generated in the following ways: (i) addition of 1.0 equiv of $NaBH_4$ in 20 μL of DMF at 233 K; (ii) passage of H_2(g) through solutions of the reduced complexes in the presence of small amounts (~0.2 equiv) of NaOH in 5 μL of DMF/ethanol.

Results and Discussion

The reaction of $[Ni(terpy)Cl_2]$ with $2,4,6\text{-}(Me)_3C_6H_2Se^-$ in an ethanol/acetonitrile mixture affords the distorted trigonal bipyramidal (TBP) complex $[Ni(terpy)(2,4,6\text{-}(Me)_3C_6H_2Se)_2]$ (**7**, Figure 1). The steric bulk of the methyl groups on the phenyl rings of the selenolates allows isolation of the monomeric pentacoordinated complex **7**. Similar TBP complexes of the new ligand DAPA, namely, $[Ni(DAPA)(SPh)_2]$ (**8**, Figure 2) and $[Ni(DAPA)(SePh)_2]$ (**9**, Figure 3), are obtained in the reaction of $[Ni(DAPA)Cl_2]$ with PhS^- or $PhSe^-$ in acetonitrile. Free rotation of the phenyl rings of DAPA appears to provide enough steric hindrance around the nickel center to give rise to the pentacoordinated complexes **8** and **9** with both PhS^- and $PhSe^-$. With the more compact terpy ligand, both PhS^- and $PhSe^-$ afford bridged dimers, and this necessitated the use of 2,4-di- and 2,4,6-trialkyl-substituted benzenethiolates and -selenolates in our previous attempts.[10,14] It is now clear that pentacoordinated Ni(II) complexes with open sixth sites could be isolated with simple thiolates and selenolates if enough steric constraints are provided through proper design of the 3N donor ligand.

Structure of $[Ni(terpy)(2,4,6\text{-}(Me)_3C_6H_2Se)_2]$ (7). A computer-generated drawing of the complex is shown in Figure 1, and selected bond distances and angles are included in Table 2. Overall, the structure of **7** is very similar to that of $[Ni(terpy)(2,4,6\text{-}(i\text{-}Pr)_3C_6H_2S)_2]$ (**2**) or $[Ni(terpy)(2,6\text{-}(Me)_2C_6H_3S)_2]$ (**3**).[10] The coordination geometry around nickel is distorted trigonal bipyramidal with the two bulky selenolate ligands in the equatorial plane. The central nitrogen of the terpy ligand is the third donor atom in this plane, while the other two nitrogens of terpy occupy the axial positions. In the crystal lattice, discrete five-coordinated molecules of **7** exist with no additional bridging interaction from neighboring Se atoms. The molecular packing is dominated by inversion-related π-stacking of the terpy planes separated by 3.319 Å.

The average Ni−Se distance (2.440(3) Å) in **7** happens to be identical to that predicted for the biological [NiSe] site (2.44 Å).[21] Interestingly, the Ni−Se bond distance in the tetrahedral complex $[Ni(dmp)(2,4,6\text{-}(Me)_3C_6H_2Se)_2]$ (**5**, 2.364(1) Å, average value) is comparatively shorter, as is the Ni−Se distance in the homoleptic square planar complex $[Ni(SeCH_2CH_2Se)_2]^{2-}$ (2.306(1) Å).[22] The average Ni−N distance in **7** (2.063(5) Å) compares well with that observed in **2**, **3**, and other terpy complexes.[10,20] In **7**, the average Se−Ni−Se angle (129.2(1)°) deviates from the ideal angle of 120° due to steric hindrance imposed by the ortho methyl groups of the selenolate ligands. This Se−Ni−Se angle is slightly smaller than the S−Ni−S angle (135.1(1)°) in **3** presumably due to the longer Ni−Se distance (2.44 Å compared to the Ni−S distance of 2.31 Å in **3**).

Structure of $[Ni(DAPA)(SPh)_2]\cdot CH_3CN$ ($8\cdot CH_3CN$). The structure consists of discrete pentacoordinated $[Ni(DAPA)(SPh)_2]$ units with acetonitrile molecules of crystallization. The closest intermolecular contacts are between the hydrogens of the methyl groups of the DAPA ligand of one molecule and the coordinated S atoms of the neighboring molecule (2.71−2.81 Å). The acetonitrile molecules are noncoordinating (closest approaches of N to the nickel centers: 5.21−5.77 Å). There are two very similar $[Ni(DAPA)(SPh)_2]$ molecules in the crystal lattice. Their overall geometries differ only by 2−5° tilts of the phenyl rings of the thiolates with respect to the NCCNCCN plane of the DAPA ligand (46.7° and 55.8° in molecule 1; 46.3° and 50.8° in molecule 2). A computer-generated drawing of **8** (molecule 1 without the acetonitrile molecule) is shown in Figure 2, and selected bond distances and angles are listed in Table 2.

In **8**, the coordination geometry around nickel is distorted trigonal bipyramidal with the two thiolate ligands in the equatorial plane. The three nitrogens of the DAPA ligand occupy the remaining coordination sites. The average Ni−N distance (2.064(5) Å) in **8** is close to that reported for $[Ni(DAPA)(NO_3)_2]$ (2.046(4) Å).[23] The terminal Ni−N bond distances of the NNN terdentate donor (mean of Ni−N(1) and Ni−N(3), 2.120(6) Å) are somewhat longer than the central Ni−N(2) bond length (1.936(5) Å); an exactly analogous situation is found in the terpy complexes.[10,20] The average Ni−S distance in **8** (2.310(2) Å) compares well with that observed in analogous TBP complexes **1**−**3**. A considerably high degree of steric interaction in the equatorial plane of **8** due to free rotation of the phenyl rings is evidenced by the S−Ni−S angle (~139°), which is larger than the S−Ni−S angles observed with the terpy complexes (130−135°).

(21) In the dimeric complex $[Ni(DMP)(PhSe)_2]_2\cdot 2CH_3CN$ (**6**), the geometry around each Ni is distorted TBP and the average Ni−Se bond distance (2.436(1) Å) is also very close to the Ni−Se distance predicted for the *D. baculatus* enzyme.

(22) Marganian, C. A.; Baidya, N.; Olmstead, M. M.; Mascharak, P. K. *Inorg. Chem.* **1992**, *31*, 2992.

(23) Alyea, E. C.; Ferguson, G.; Restivo, R. J. *Inorg. Chem.* **1975**, *14*, 2491.

Table 1. Summary of Crystal Data, Intensity Collection, and Structure Refinement Parameters for [Ni(terpy)(2,4,6-$(Me)_3C_6H_2Se)_2$] (**7**), [Ni(DAPA)$(SPh)_2$]·CH_3CN (**8**·CH_3CN), and [Ni(DAPA)$(SePh)_2$]·CH_3CN (**9**·CH_3CN)

	7	**8**·CH_3CN	**9**·CH_3CN
formula (mol wt)	$C_{33}H_{33}N_3NiSe_2$ (687.9)	$C_{35}H_{32}N_4NiS_2$ (631.5)	$C_{35}H_{32}N_4NiSe_2$ (725.3)
color and habit	dark plates	red brown plates	brown needles
cryst syst	monoclinic	monoclinic	monoclinic
space group	$P2_1/n$	$P2_1/c$	$P2_1/c$
a, Å	13.170(6)	23.012(7)	23.209(2)
b, Å	16.091(5)	17.814(5)	17.960(1)
c, Å	15.111(8)	15.698(4)	15.749(1)
β, deg	114.42(2)	108.52(2)	108.482(6)
V, Å^3	2916(2)	6099(5)	6225(8)
Z	4	8	8
cryst dimens, mm	0.08 × 0.20 × 0.24	0.16 × 0.24 × 0.52	0.08 × 0.08 × 0.30
d_{calcd} (130 K), g cm^{-3}	1.568	1.375	1.547
μ, mm^{-1}	4.015[a]	0.805[b]	3.806[a]
transm coeff	0.49−0.76	0.82−0.90	0.66−0.78
scan method	$\theta-2\theta$	ω, 1.0° range	$\theta-2\theta$
2θ range, deg	0.0−108.5	0−50	0.0−108.5
no. of data collected	3909	11611	8845
no. of data used in refinement ($I > 4\sigma(I)$)	2730	6133	5808
no. of parameters refined	351	727	757
R,[c] %	4.78	6.46	3.90
R_w,[d] %	5.05	5.40	3.77
GOF	1.26	1.19	1.16
largest Δ/σ	0.027	0.002	0.013
largest difference peak, e Å^{-3}	0.75	0.57	0.45

[a] Cu Kα (λ = 1.541 78 Å). [b] Mo Kα (λ = 0.710 73 Å). [c] $R = \sum||F_o| - |F_c||/|F_o|$. [d] $R_w = \sum||F_o| - |F_c||w^{1/2}/\sum|F_o w^{1/2}|$.

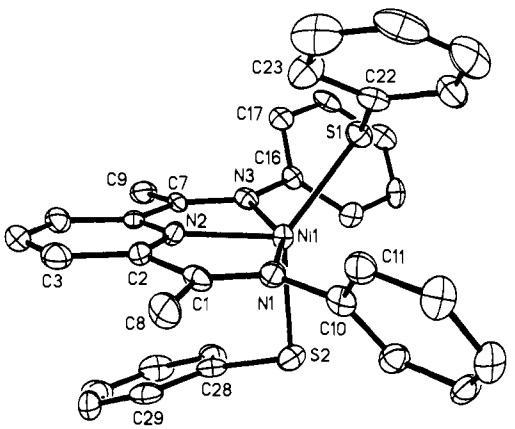

Figure 2. Thermal ellipsoid plot (50% probability level) of **8** (molecule 1 without the acetonitrile molecule) with the atom-labeling scheme. Hydrogen atoms are omitted for clarity.

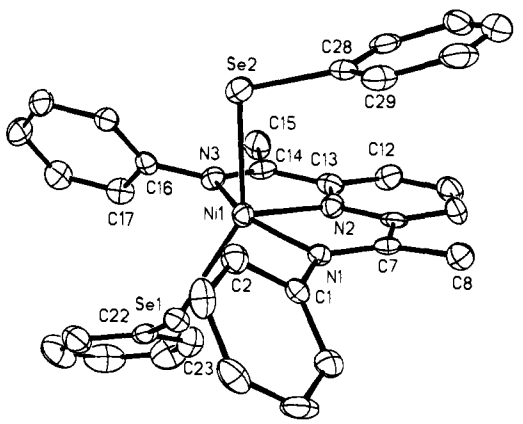

Figure 3. Thermal ellipsoid plot (50% probability level) of **9** (molecule 1 without the acetonitrile molecule) with the atom-labeling scheme. Hydrogen atoms are omitted for clarity.

Structure of [Ni(DAPA)$(SePh)_2$]·CH_3CN (9·CH_3CN). The complexes **8** and **9** are isostructural. Discrete pentacoordinated [Ni(DAPA)$(SePh)_2$] units and noncoordinating acetonitrile molecules comprise the crystal structure. Dominant intermolecular contacts exist between the methyl hydrogens and the Se(1) centers of neighboring units (2.85−2.88 Å), while two phenyl hydrogens enclose Se(2) intramolecularly at distances of 3.05 and 2.72 Å. Here again, two very similar [Ni(DAPA)-$(SePh)_2$] molecules are present in the crystal lattice. Their overall geometries differ only by 2−5° tilts of the phenyl rings of the selenolates with respect to the NCCNCCN plane of the DAPA ligand (46.7° and 55.8° in molecule 1; 46.3° and 50.8° in molecule 2). A computer-generated drawing of **9** (molecule 1 without the acetonitrile molecule) is shown in Figure 3, and selected bond distances and angles are listed in Table 2. The metric parameters of **9** compare well with those of analogous compounds. For example, the average Ni−N distance (2.059(5) Å) is very close to that in **8**, while the average Ni−Se distance (2.420(1) Å) is nearly identical to that observed in **7**.

Properties. The complexes **7**−**9** are sensitive to oxygen, the Se-containing complexes **7** and **9** being more sensitive than **8** and analogous thiolato complexes. The room temperature (298 K) magnetic susceptibility values of polycrystalline **7** (3.32 μ_B), **8** (2.89 μ_B), and **9** (3.15 μ_B) are consistent with distorted TBP geometries with two unpaired electrons at the Ni(II) centers. The complex **7** dissolves in aprotic solvents like DMSO and DMF to give dark purple solutions, while dark brown solutions are obtained with **8** and **9** in these solvents. The electronic absorption spectra of all three complexes exhibit several broad and overlapping bands of very different intensities. Presently, no attempt has been made to assign these spectra. The ^{1}H NMR spectrum of **7** in $(CD_3)_2SO$ exhibits six isotropically shifted resonances at 165.80, 78.28, 74.72, 49.62, 23.01, and 17.46 ppm (from TMS) due to the coordinated terpy ligand (Figure 4). The four meta hydrogens of the two selenolates resonate at 18.40 ppm, and the methyl group hydrogens on the benzene rings give rise to peaks at 27.44 (p-CH_3) and 17.16 (o-CH_3) ppm. Between the DAPA complexes, only **9** is soluble enough in $(CD_3)_2SO$ to afford a well-resolved ^{1}H NMR spectrum in which the six resonances of the DAPA ligand appear at 79.57, 24.25, 14.34, −8.11, −22.75, and −24.93 ppm (from TMS).[24] The four meta hydrogens of the coordinated phenylselenolates resonate at 15.85 ppm, while the ortho and para hydrogens (total six) of the same two ligands appear as a broad peak at −13.38 ppm.[25] The clean

(24) [Ni(DAPA)Cl_2] in $(CD_3)_2SO$ exhibits these six peaks at 78.01, 18.66, 13.82, −3.34, −6.06, and −7.89 ppm (from TMS).

Table 2. Selected Bond Distances (Å) and Angles (deg) for **7**–**9**

[Ni(terpy)(2,4,6-(Me)$_3$C$_6$H$_2$Se)$_2$] (7)			
Ni–Se(1A)	2.507(3)	Ni–Se(1B)	2.426(3)
Ni–Se(2)	2.387(2)	Ni–N(1)	2.109(5)
Ni–N(2)	1.976(6)	Ni–N(3)	2.106(5)
Se(1A)–C(16)	1.935(6)	Se(1B)–C(16)	1.941(6)
Se(2)–C(25)	1.930(7)	N(1)–C(1)	1.336(9)
N(2)–C(6)	1.341(8)	N(3)–C(11)	1.382(10)
C(1)–C(2)	1.375(9)	C(5)–C(6)	1.469(10)
C(10)–C(11)	1.481(9)	C(16)–C(17)	1.395(11)
C(25)–C(26)	1.399(11)	C(26)–C(31)	1.505(10)
Se(1A)–Ni–Se(2)	132.2(1)	Se(1B)–Ni–Se(2)	126.3(1)
Se(1A)–Ni–N(1)	93.6(2)	Se(1B)–Ni–N(1)	93.5(2)
Se(2)–Ni–N(1)	97.8(2)	Se(1A)–Ni–N(2)	105.8(2)
Se(1B)–Ni–N(2)	111.8(2)	Se(2)–Ni–N(2)	121.9(2)
N(1)–Ni–N(2)	78.4(2)	N(1)–Ni–N(3)	156.7(3)
N(2)–Ni–N(3)	78.4(2)	Ni–Se(1A)–C(16)	103.0(3)
Ni–Se(1B)–C(16)	105.7(3)	Ni–Se(2)–C(25)	109.2(3)
Ni–N(1)–C(1)	127.7(5)	Ni–N(2)–C(6)	119.7(5)
Ni–N(2)–C(10)	119.6(4)	C(25)–C(26)–C(31)	121.8(6)
[Ni(DAPA)(SPh)$_2$]·CH$_3$CN (**8**·CH$_3$CN)			
Ni(1)–N(1)	2.110(7)	Ni(1)–N(2)	1.936(5)
Ni(1)–N(3)	2.131(6)	Ni(1)–S(1)	2.263(2)
Ni(1)–S(2)	2.351(2)	N(1)–C(1)	1.293(9)
N(1)–C(10)	1.431(10)	N(2)–C(2)	1.339(10)
N(3)–C(16)	1.417(9)	S(1)–C(22)	1.768(8)
S(2)–C(28)	1.764(8)	C(1)–C(8)	1.493(11)
C(7)–C(9)	1.495(11)	C(10)–C(11)	1.388(11)
C(16)–C(17)	1.397(10)	Ni(2)–N(4)	2.129(5)
Ni(2)–N(5)	1.933(5)	Ni(2)–N(6)	2.138(5)
Ni(2)–S(3)	2.265(2)	Ni(2)–S(4)	2.362(2)
N(4)–C(34)	1.312(9)	N(4)–C(43)	1.429(8)
N(5)–C(35)	1.352(8)	N(5)–C(39)	1.340(8)
N(6)–C(40)	1.292(8)	N(6)–C(49)	1.425(9)
S(3)–C(55)	1.766(6)	S(4)–C(61)	1.763(6)
C(35)–C(36)	1.395(10)	C(40)–C(42)	1.492(8)
C(43)–C(44)	1.397(9)	C(55)–C(56)	1.399(10)
N(1)–Ni(1)–N(2)	78.3(2)	N(1)–Ni(1)–N(3)	156.4(2)
N(2)–Ni(1)–N(3)	78.1(2)	N(1)–Ni(1)–S(1)	100.9(1)
N(2)–Ni(1)–S(1)	123.6(2)	N(3)–Ni(1)–S(1)	90.5(1)
N(1)–Ni(1)–S(2)	92.5(1)	N(2)–Ni(1)–S(2)	97.8(2)
N(3)–Ni(1)–S(2)	92.7(1)	S(1)–Ni(1)–S(2)	138.2(1)
Ni(1)–N(1)–C(1)	114.8(5)	Ni(1)–N(1)–C(10)	124.3(5)
C(1)–N(1)–C(10)	120.8(7)	C(7)–N(3)–C(16)	123.5(6)
N(1)–C(1)–C(2)	113.8(7)	C(2)–C(1)–C(8)	119.2(6)
N(3)–C(7)–C(6)	114.7(6)	C(6)–C(7)–C(9)	119.8(6)
N(1)–C(10)–C(11)	122.6(6)	N(3)–C(16)–C(17)	121.8(6)
C(16)–C(17)–C(18)	119.0(6)	C(28)–C(29)–C(30)	120.7(7)
N(4)–Ni(2)–N(5)	78.6(2)	N(4)–Ni(2)–N(6)	156.1(2)
N(5)–Ni(2)–N(6)	77.7(2)	N(4)–Ni(2)–S(3)	100.8(2)
N(5)–Ni(2)–S(3)	121.7(2)	N(6)–Ni(2)–S(3)	89.5(2)
N(4)–Ni(2)–S(4)	92.9(2)	N(5)–Ni(2)–S(4)	98.4(2)
N(6)–Ni(2)–S(4)	93.0(2)	S(3)–Ni(2)–S(4)	139.3(1)
Ni(2)–N(4)–C(34)	113.8(4)	Ni(2)–N(4)–C(43)	124.7(4)
Ni(2)–N(6)–C(40)	114.1(4)	Ni(2)–N(6)–C(49)	123.4(4)
Ni(2)–S(3)–C(55)	112.2(3)	Ni(2)–S(4)–C(61)	104.9(3)
N(4)–C(34)–C(41)	125.7(6)	C(35)–C(34)–C(41)	119.7(6)
N(5)–C(39)–C(40)	114.0(6)	C(39)–C(40)–C(42)	118.3(6)
[Ni(DAPA)(SePh)$_2$]·CH$_3$CN (**9**·CH$_3$CN)			
Ni(1)–Se(1)	2.374(1)	Ni(1)–Se(2)	2.466(1)
Ni(1)–N(1)	2.124(5)	Ni(1)–N(2)	1.939(5)
Ni(1)–N(3)	2.114(5)	Se(1)–C(22)	1.919(6)
Se(2)–C(28)	1.920(6)	N(1)–C(1)	1.428(8)
N(2)–C(13)	1.327(8)	N(3)–C(16)	1.429(8)
C(1)–C(2)	1.386(8)	C(7)–C(8)	1.496(9)
C(12)–C(13)	1.399(8)	C(13)–C(14)	1.487(9)
C(14)–C(15)	1.492(10)	C(16)–C(17)	1.392(8)
Se(1)–Ni(1)–Se(2)	137.8(1)	Se(1)–Ni(1)–N(1)	90.0(1)
Se(2)–Ni(1)–N(1)	92.7(1)	Se(1)–Ni(1)–N(2)	124.6(1)
Se(2)–Ni(1)–N(2)	97.1(1)	N(1)–Ni(1)–N(2)	78.2(2)
Se(1)–Ni(1)–N(3)	101.3(1)	Se(2)–Ni(1)–N(3)	92.4(1)
N(1)–Ni(1)–N(3)	156.6(2)	N(2)–Ni(1)–N(3)	78.5(2)
Ni(1)–Se(1)–C(22)	108.3(2)	Ni(1)–Se(2)–C(28)	102.9(2)
N(1)–C(1)–C(2)	118.3(5)	N(1)–C(7)–C(8)	127.5(6)
N(2)–C(13)–C(12)	119.5(6)	N(3)–C(14)–C(15)	126.6(6)
C(16)–C(17)–C(18)	119.0(5)	Se(1)–C(22)–C(23)	121.3(5)
C(22)–C(23)–C(24)	121.7(6)	Se(2)–C(28)–C(29)	121.3(5)

NMR spectra of the present complexes confirm the presence of the desired mononuclear Ni(II) species in DMSO (and DMF) solution.

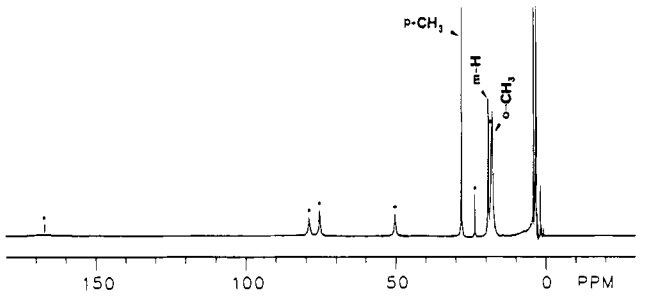

Figure 4. ^{1}H NMR spectrum (300 MHz, 298 K) of **7** in $(CD_3)_2SO$. Signal assignments for the protons of the selenolate ligands are indicated. The six sets of terpy resonances are marked with asterisks.

Redox Behaviors and Substrate Binding Studies. The DAPA complexes **8** and **9** comprise the first set of synthetic analogues of the biological nickel site that undergo reversible redox transformations with biologically relevant oxidants and reductants.[26] This unique property has allowed us to (a) produce genuine Ni(III) and Ni(I) complexes containing the $[NiN_3E_2]$ (E = S, Se) chromophore, (b) study their affinities toward CO, H^-, and H_2, and (c) compare the EPR parameters of such species with those of the various nickel signals of the enzyme. As described below, results of such experiments have enabled us to assign more reliably the redox state of the nickel center in the catalytically active Ni-C form of the enzyme. A preliminary account of the redox properties of **8** has already appeared.[15] Here we report the redox behavior of **8** in detail (Scheme 1) and compare it with that of **9** (Scheme 2) to determine the differences in reactivities due to the presence of Se in place of S in the coordination sphere of nickel. The redox properties of **7** are also included to determine such differences in case of the terpy complexes. Also, among the TBP terpy complexes, **7** reacts more readily with H_2; hence this terpy analogue has been included in the present account. Since samples for low-temperature EPR measurements are required to form good glasses, DMF has been used as the solvent though similar results have also been obtained in DMSO solutions.

(a) [Ni(DAPA)(SPh)$_2$] (8). Unlike its terpy analogue,[10] oxidation of **8** to $[Ni^{III}(DAPA)(SPh)_2]^+$ (**10**) is readily achieved in DMF (233–253 K) with $(Et_4N)_3[Fe(CN)_6]$ (Scheme 1). The Ni(III) complex **10** is characterized by an axial EPR spectrum with $g_\perp = 2.214$ and $g_\parallel = 2.032$ with a five-line hyperfine splitting pattern ($A = 14.5$ G) in the $g = 2.032$ region. These features indicate that the single unpaired electron on nickel resides in the d_{z^2} orbital ($g_\perp > g_\parallel$)[27] and interacts with the two axial N ($I = 1$) donor atoms of the DAPA ligand. Reduction of **8** in DMF by aqueous $Na_2S_2O_4$ in DMF (295 K) produces the reduced species $[Ni^I(DAPA)(SPh)_2]^-$ (**11**), which exhibits

(25) In the ^{1}H NMR spectrum of $[Ni(terpy)(PhSe)_2]_2$ (**4**) in $(CD_3)_2SO$, the ortho and para hydrogens of the coordinated benzeneselenolates also appear together as a broad peak at −13.20 ppm (from TMS).

(26) The starting materials ($[Ni(terpy)Cl_2]$ and $[Ni(DAPA)Cl_2]$) and the solvated species like $[Ni(terpy)(solv)_2]$ are all redox active and give rise to complicated voltammograms. The intrinsic redox activities in these control experiments prevented unambiguous determination of the redox parameters of the terpy and DAPA complexes with $[NiN_3E_2]$ (E = S, Se) chromophores. The voltammograms of the model complexes were always very complicated, and several waves (some quasireversible ones) were recorded. Also, solvolysis of the thiolate and selenolate complexes during the redox cycles invariably afforded additional species in solution. It is difficult to sort out the parameters for the *metal-centered redox processes of the desired complexes* in such situations. We have therefore sought chemical means of generating the Ni(I) and Ni(III) species in the present work.

(27) (a) Lappin, A. G.; McAuley, A. *Adv. Inorg. Chem.* **1988**, *32*, 241. (b) Salerno, J. C. In *The Bioinorganic Chemistry of Nickel*; Lancaster, J. R., Jr., Ed.; VCH Publishers: Deerfield Beach, FL, 1988; Chapter 3, p 53. (c) Nag, K.; Chakravorty, A. *Coord. Chem. Rev.* **1980**, *33*, 87.

Scheme 1

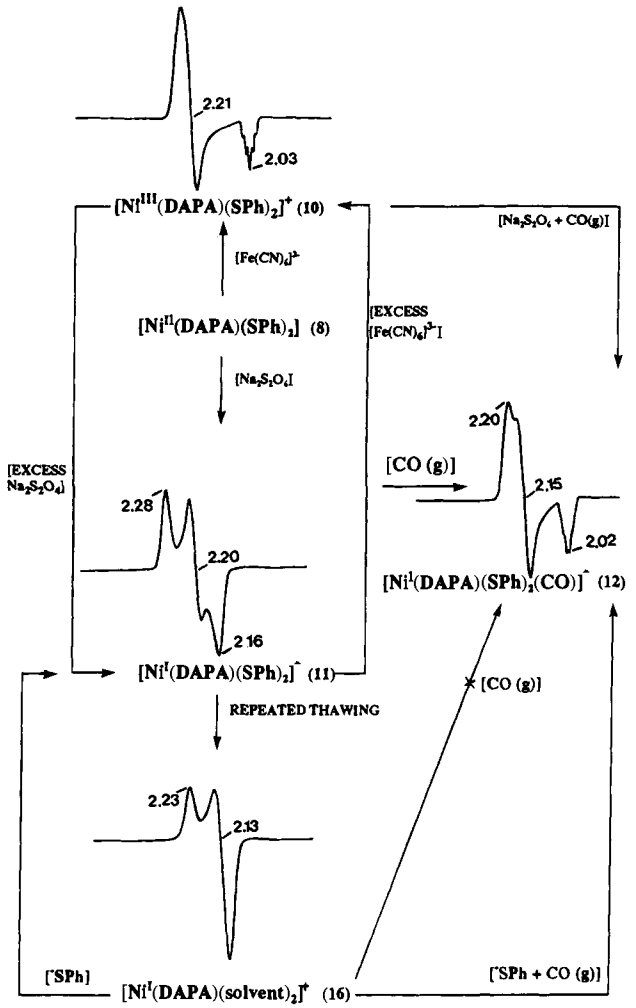

Scheme 2

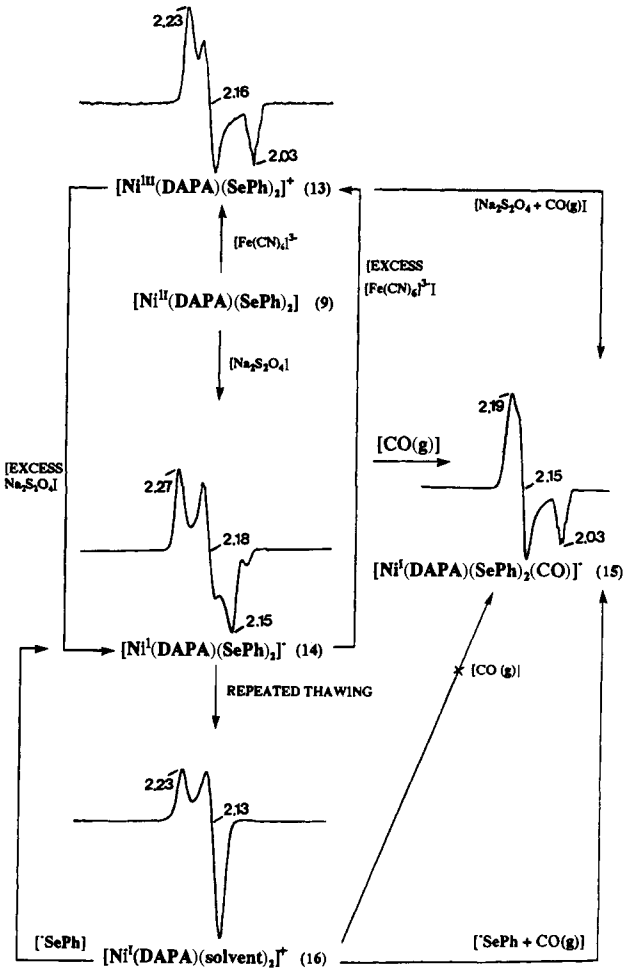

an EPR signal with $g = 2.283, 2.201$, and 2.164. The unpaired electron in **11** resides in the $d_{x^2-y^2}$ orbital ($g_\perp < g_\parallel$).[27] Only the reduced (Ni(I)) complex **11** binds CO to produce the CO adduct $[Ni^I(DAPA)(SPh)_2(CO)]^-$ (**12**), which also exhibits a rhombic EPR spectrum ($g = 2.198, 2.145, 2.023$) with five-line hyperfine splitting (A = 13 G) at g = 2.023. The Ni(I)-CO adduct $[Ni^I(DAPA)(SPh)_2(CO)]^-$ (**12**), generated in DMF solution, displays ν_{CO} at 2040 cm^{-1}. This CO stretching frequency is close to those exhibited by the Ni(I) complexes of tris[(*tert*-butylthio)ethyl]amine (NS_3^{tBu}) $[Ni(NS_3^{tBu})CO]^+$ (2026 cm^{-1})[28] and tetraazamacrocycles with four imine nitrogens (2020 cm^{-1}).[29]

(b) [Ni(DAPA)(SePh)$_2$] (9). Oxidation of **9** to $[Ni^{III}(DAPA)(SePh)_2]^+$ (**13**) with $(Et_4N)_3[Fe(CN)_6]$ (Scheme 2) proceeds smoothly in DMF at subzero temperatures (233–253 K). **13** displays a more rhombic EPR spectrum (g = 2.225, 2.163, 2.033) with the same five-line hyperfine coupling with A = 14.5 G on the g = 2.033 line, indicating interaction of the single electron in the d_{z^2} orbital with the two axial N atoms. Unlike **10**, **13** is not very stable at low temperature. Reduction of **9** in DMF by aqueous $Na_2S_2O_4$ (295 K) affords the reduced species $[Ni^I(DAPA)(SePh)_2]^-$ (**14**) with the unpaired electron in the $d_{x^2-y^2}$ orbital. **14** gives rise to an EPR signal with g = 2.269, 2.184, and 2.151. Much like **11**, **14** binds CO (Scheme 2) to give $[Ni^I(DAPA)(SePh)_2(CO)]^-$ (**15**, g = 2.188, 2.145, 2.027; A = 13 G at g = 2.027; ν_{CO} = 2024 cm^{-1}). Binding of CO to **11** and **14** is a reversible process; passage of dinitrogen through solutions of the CO adducts **12** and **15** regenerates the reduced species **11** and **14**.

Schemes 1 and 2 reveal few trends in the reactivities of the Ni(III) and Ni(I) species derived from **8** and **9**. The most prominent one is the reversible nature of the Ni(III) ⇌ Ni(II) ⇌ Ni(I) transformations. Addition of a slight excess of $Na_2S_2O_4$ to the Ni(III) complexes **10** and **13** readily affords the corresponding Ni(I) species **11** and **14**, while reaction of excess $(Et_4N)_3[Fe(CN)_6]$ with **11** and **14** produces the oxidized complexes **10** and **13** in high yields. In each case, an EPR-silent Ni(II) intermediate is detected upon stepwise addition of the oxidant or reductant. Though these redox transformations are facilitated at low temperatures, the three biologically relevant redox states of nickel are readily attainable in **8** and **9**, and in this sense, these two DAPA complexes are functionally one step closer to the biological nickel site. The yields of the redox reactions, as judged by the intensity of the EPR signals, fall in the range 50–80% when performed at subzero temperatures. In general, the reduced species are thermally more stable compared to the oxidized species. For example, **11** is moderately stable at ice temperature and even at room temperature for several hours. Another important trend to note in Schemes 1 and 2 is the affinity of CO to the Ni(I) species only. Both **10** and **13** fail to bind CO under very high partial pressures of CO, a fact that confirms that CO has no affinity for the Ni(III) center. Also, stepwise oxidation of **12** or **15** with $[Fe(CN)_6]^{3-}$ first generates an EPR-silent species and then the oxidized complex **10** or **13** (Figure S1, supplementary material). It is thus clear that even coordinated CO in **12** or **15** dissociates from the nickel center upon oxidation. Chemically, this is expected since CO is a better π-acceptor for metals in low oxidation states.

(28) Stavropoulos, P.; Muetterties, M. C.; Carrie, M.; Holm, R. H. *J. Am. Chem. Soc.* **1991**, *113*, 8485.
(29) Gagne, R. R.; Ingle, D. M. *Inorg. Chem.* **1981**, *20*, 420.

Another important characteristic of the reaction of CO with the Ni(I) centers in **11** and **14** is its reversibility. Gradual formation of the CO adducts **12** and **15** upon passage of CO through solutions of the reduced species in DMF can be easily monitored by EPR spectroscopy. Both **12** and **15** are quite stable and can be stored for days at low temperatures. However, when dinitrogen is passed through solutions of these CO adducts, the Ni(I) complexes (**11** and **14**) are regenerated within minutes. These results confirm that CO binds to the Ni(I) centers reversibly. Reversible CO binding to the nickel centers of the reduced terpy analogues has been reported previously by this group.[10]

Repeated thawing of the frozen solutions of **11** and **14** results in the loss of thiolate/selenolate ligands from the Ni(I) centers. This is evidenced by the appearance of a new axial EPR spectrum of $[Ni^{I}(DAPA)(solv)_2]^+$ (**16**) with $g = 2.228$ and 2.130 (Schemes 1 and 2). The facts that (a) both **11** and **14** eventually afford the same EPR spectrum and (b) addition of thiolate or selenolate to **16** gives rise to **11** or **14** confirm that **16** is indeed the solvated Ni(I) complex of the DAPA ligand. Upon reduction with aqueous $Na_2S_2O_4$ at 295 K, $[Ni(DAPA)Cl_2]$ also produces a stable Ni(I) species, presumably $[Ni^{I}(DAPA)Cl_2]^-$, which exhibits a very similar axial EPR spectrum with $g = 2.270$ and 2.150. Repeated thawing of the $[Ni^{I}(DAPA)Cl_2]^-$ sample in the presence of aqueous $Na_2S_2O_4$ does not bring about any change in its EPR spectrum. This latter observation confirms that the changes in the EPR spectrum of **11** or **14** upon prolonged thawing are indeed due to the loss of the thiolate/selenolate ligands and not to any chemical change in the DAPA ligand framework. It is also important to note that while CO does not bind to **16** alone, it does so in the presence of 2 equiv of thiolate or selenolate (Schemes 1 and 2). Along the same line, CO binds to $[Ni^{I}(DAPA)Cl_2]^-$ only in the presence of 2 equiv of thiolate/selenolate ligand. It is therefore evident that CO-binding to the Ni(I) centers is possible only when electron-rich S or Se donors are present in the first coordination sphere. Taken together, these observations indicate that the loss of the thiolate/selenolate ligands from the Ni(I) centers is at least partly due to excessive charge buildup at the metal centers which can be alleviated by the addition of a π-accepting ligand like CO.

As mentioned earlier, the change from the terpy to the DAPA ligand system was intended to provide moderate stability to both Ni(I) and Ni(III) species. The observations mentioned above clearly indicate that the objective has indeed been achieved. The terpy ligand framework provides more stability to the Ni(I) species presumably due to its ability to delocalize electron density over the ligand π system. As a result, no loss of thiolate or selenolate (vide infra) ligands due to excessive charge buildup at the metal center occurs with the Ni(I)–terpy complexes upon prolonged thawing.[10] The DAPA ligand, on the other hand, is less effective in removing electron density from the Ni(I) centers; hence loss of thiolate/selenolate ligands is observed. By the same token, DAPA provides a better ligand framework for the Ni(III) centers. Thus more stable Ni(III) species are obtained with the DAPA ligand (present work), while oxidations of the terpy complexes always proceed marginally with unstable Ni(III) species as the final products.

The CO stretching frequencies of the CO adducts of the various Ni(I) species are good indicators of the electron density at the Ni(I) centers.[30] Since $[Ni^{I}(DAPA)(SPh)_2(CO)]^-$ (**12**) exhibits a slightly higher ν_{CO} (2040 cm^{-1}) compared to $[Ni^{I}(DAPA)(SePh)_2(CO)]^-$ (**15**) ($\nu_{CO} = 2024$ cm^{-1}), it is evident that, between PhS^- and $PhSe^-$, the thiolate ligand donates less electron density to the nickel(I) centers. This is expected on the basis of the comparatively "harder" nature of the RS^- ligand. A much faster loss of the thiolate ligands from $[Ni^{I}(DAPA)(SPh)_2]^-$ (**11**) compared to the loss of selenolates from $[Ni^{I}(DAPA)(SePh)_2]^-$ (**14**) also supports this notion.[31]

[Ni(terpy)(2,4,6-$(Me)_2C_6H_2Se)_2$] (7). The redox and chemical reactivities of **7** resemble those of the terpy analogues with the NiN_3S_2 chromophore.[10] Reduction of **7** to $[Ni^{I}(terpy)(2,4,6\text{-}(Me)_3C_6H_2Se)_2]^-$ (**17**) is achieved in DMF (295 K) by aqueous $Na_2S_2O_4$. **17** exhibits an axial EPR signal with $g_{\|} = 2.250$ and $g_{\perp} = 2.103$. Passage of CO through a solution of **17** gives rise to $[Ni^{I}(terpy)(2,4,6\text{-}(Me)_3C_6H_2Se)_2(CO)]^-$ (**18**, $g = 2.204$, 2.131, 2.024). The binding of CO to **17** is reversible. Much like the other terpy analogues, oxidation of **7** produces samples that display very weak EPR signals ($g = 2.242$, 2.211, 2.046) and are not amenable to further binding studies.

Reactions with Hydride (H^-). Kinetic studies on hydrogen activation by H_2ases indicate that the process involves heterolytic cleavage of H_2 with the possible formation of a metal hydride ($M-H^-$) species as the intermediate that gives rise to the Ni-C signal.[11c,32] This idea has been supported by photolysis studies on the H_2-reduced enzyme.[6,33] as well as by ^1H and ^2H Q-band ENDOR experiments.[34] Since the enzyme exhibits the Ni-C signal under reducing conditions, it is chemically reasonable to assign a Ni(I)–hydride formalism to the species responsible for this signal. This hypothesis is supported by the fact that good structural models like the terpy complexes **2** and **3** form hydride adducts in their reduced forms and exhibit EPR spectra very similar to the Ni-C signal of the H_2ases.[10] We now report that the present three complexes **7**–**9** readily bind hydride in their reduced forms and exhibit EPR spectra much like the Ni-C signal. Among all the model complexes with the NiN_3E_2 (E = S, Se) chromophore, the DAPA complexes **8** and **9** clearly exhibit superior hydride-binding capabilities.

(a) [Ni(DAPA)$(SPh)_2$] (8) and [Ni(DAPA)$(SePh)_2$] (9). At 233 K, the complexes **8** and **9** react with $NaBH_4$ in DMF to afford the hydride adducts $[Ni^{I}(DAPA)(SPh)_2(H^-)]^2$ (**19**, Scheme 3) and $[Ni^{I}(DAPA)(SePh)_2(H^-)]^{2-}$ (**20**, Scheme 4). $NaBH_4$ acts as both the reductant and the source of the hydride ligand in these reactions. The presence of a small amount (~0.2 equiv) of a base like NaOH increases the yield of the hydride adducts to a considerable extent (>50%, Schemes 3 and 4). If the reduced species **11** and **14** are produced with aqueous $Na_2S_2O_4$, subsequent formation of the hydride adducts **19** and **20** with additional $NaBH_4$ is only possible in the presence of a base. This indicates that the hydride adducts are more stable in basic solutions. **19** exhibits a pseudorhombic EPR signal with $g = 2.264$, 2.220, 2.035, while **20** displays a rhombic EPR spectrum with $g = 2.262$, 2.222, 2.036 (Schemes 3 and 4). The five-line hyperfine splitting pattern around $g \approx 2$($A = 14.5$ G) in both of these spectra indicates that in **19** and **20**, the unpaired electron occupies the d_{z^2} orbital and interacts with two N ($I = 1$) nuclei at the axial positions. Binding of hydride at the sixth site of **11** and **14** therefore converts the $d_{x^2-y^2}$ ground state to d_{z^2} presumably by changing the relative positions of the d orbitals following conversion of the TBP species into the octahedral

(30) In case of the terpy complexes (**1**–**3**) reported previously, $[Ni^{I}(terpy)(C_6F_5S)_2(CO)]^-$ with electron-withdrawing thiolates exhibits ν_{CO} at 2045 cm^{-1}, a value higher than the ν_{CO} of $[Ni^{I}(terpy)(2,6\text{-}(Me)_2C_6H_3S)_2(CO)]^-$ at 2035 cm^{-1}.

(31) The higher yields and stability of the Ni(III) species $[Ni^{III}(DAPA)(SPh)_2]^+$ (**10**) in comparison to $[Ni^{III}(DAPA)(SePh)_2]^+$ (**13**) are also in line with this conclusion.

(32) Lespinat, P. A.; Berlier, Y.; Fauque, G.; Czechowski, M.; Dimon, B.; LeGall, J. *Biochimie* **1986**, *68*, 55.

(33) Cammack, R.; Patil, D. S.; Hatchikian, E. C.; Fernandez, V. M. *Biochim. Biophys. Acta* **1987**, *912*, 98.

(34) (a) Whitehead, J. P.; Gurbiel, R. J.; Bagyinka, C.; Hoffman, B. M.; Maroney, M. J. *J. Am. Chem. Soc.* **1993**, *115*, 5629. (b) Fan, C.; Teixeira, M.; Moura, J.; Moura, I.; Huynh, B.-H.; LeGall, J.; Peck, H. D., Jr.; Hoffman, B. M. *J. Am. Chem. Soc.* **1991**, *113*, 20.

Scheme 3

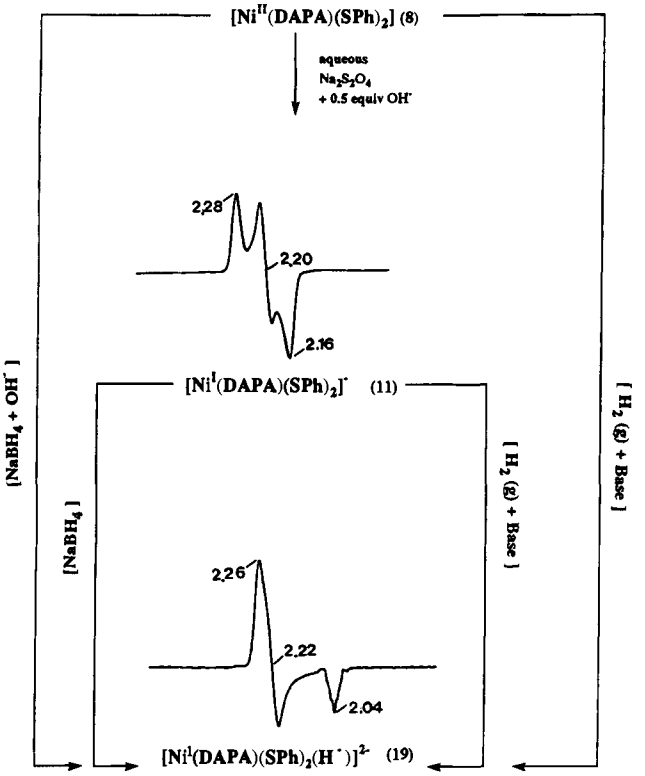

Scheme 4

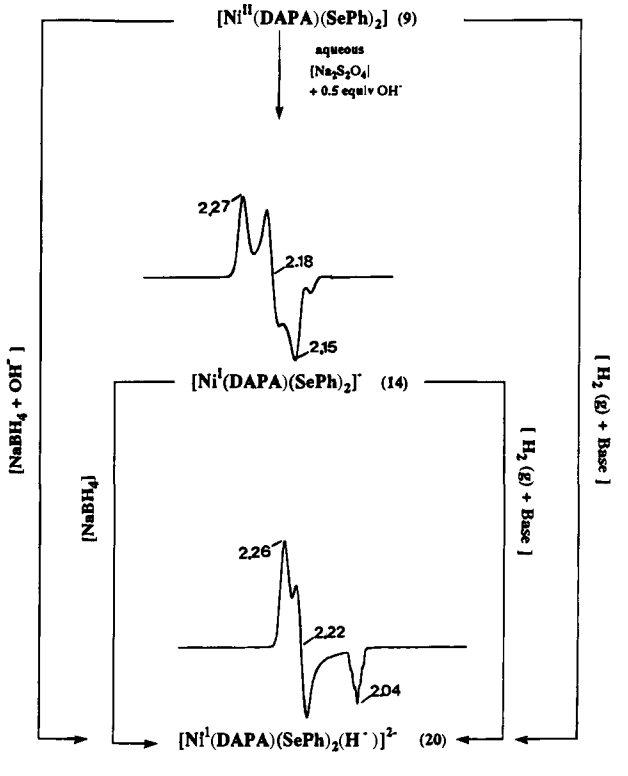

species.[10] Between the two DAPA complexes, **9** gives rise to a higher concentration of the hydride adduct (**20**) in these reactions.

(b) [Ni(terpy)(2,4,6-(Me)$_3$C$_6$H$_2$Se)$_2$] (7). Addition of $NaBH_4$ to the DMF solution of **7** at 233 K gives rise to $[Ni^I(terpy)(2,4,6\text{-}(Me)_3C_6H_2Se)_2(H^-)]^{2-}$ (**21**) in a low concentration. **21** exhibits a rhombic EPR signal with g values (2.240, 2.191, 2.047) very similar to those for $[Ni^I(terpy)(2,6\text{-}(Me)_2C_6H_3S)_2(H^-)]^{2-}$.[10] Overall, the terpy complexes afford much lower concentrations of the hydride adducts compared to the corresponding DAPA analogues.

Reactions with Hydrogen Gas. If the postulate that a Ni(I)–hydride intermediate gives rise to the Ni-C signal following incubation of the enzyme under dihydrogen is correct, then reactions of dihydrogen with the model complexes at ambient temperature should generate the Ni(I)–hydride species **19**–**21**. In the following section, we report that such reactions do take place and afford the desired Ni(I)–hydride species.

(a) [Ni(DAPA)(SPh)$_2$] (8) and [Ni(DAPA)(SePh)$_2$](9). At 298 K, passage of hydrogen gas through solutions of **8** and **9** in DMF affords samples that exhibit weak EPR spectra of the Ni(I)–hydride adducts **19** and **20** (Schemes 3 and 4). Use of activated charcoal as a suspension in such a solution enhances the intensities of the EPR signals of the hydride adducts presumably by increasing the availability of H_2 in the solution phase. Interestingly, the presence of a base like NaOH in the reaction mixtures enhances the intensities of the EPR signals to a considerable extent (Schemes 3 and 4). For example, passage of H_2 for 1 min through a 10 mM solution of **9** in DMF containing 5 mg of activated charcoal and 0.5 equiv of NaOH resulted in a sample that exhibited a strong EPR signal of the hydride adduct **20**. Spin integration experiments indicated that over 50% of the starting Ni(II) complex was converted into the hydride adduct under the reaction conditions. This reactivity is quite remarkable especially under such mild reaction conditions. Enhancement of hydride formation in the presence of a base is very encouraging in the sense that it lends support to the mechanism involving heterolytic cleavage of H_2.

The hydride adducts **19** and **20** are formed in much higher yields (as judged by the intensities of the EPR signals) when H_2 is passed through solutions of the reduced (Ni(I)) species **11** and **14** in DMF at 298 K. The presence of small amounts (~0.5 equiv) of a base like NaOH in the reaction mixtures is necessary for the formation of the hydride adducts in these cases (Schemes 3 and 4). Here also the use of activated charcoal in the reaction mixtures increases the overall yields of **19** and **20**. The presence of thiolate/selenolate ligands in the coordination sphere of Ni(I) is required for successful formation of the hydride adducts **19** and **20**. This is indicated by the failure of $[Ni^I(DAPA)Cl_2]^-$ to produce a Ni(I)–hydride adduct upon incubation with dihydrogen under basic conditions.

(b) [Ni(terpy)(2,4,6-(Me)$_3$C$_6$H$_2$Se)$_2$] (7). At 298 K, reaction of **17** with H_2 in DMF in the presence of 0.5 equiv of NaOH produces the hydride adduct $[Ni(terpy)(2,4,6\text{-}(Me)_3C_6H_2Se)_2(H^-)]^{2-}$ (**21**) in marginal yield. Since the DAPA complexes **8** and **9** exhibit significant reactivities toward H_2(g), reactions of **7** have not been studied further.

Proposed Structure of the Hydride Adducts. Binding of hydride to the Ni(I) complexes **11** and **14** results in the hexacoordinated species **19** and **20** with a d_{z^2} ground state. The five-line hyperfine splitting pattern in the $g = 2$ region of the EPR spectra of the hydride adducts clearly indicates that the two axial sites in these pseudooctahedral complexes are occupied by two N ($I = 1$) donor atoms from the DAPA ligand. Since no noticeable hyperfine splitting due to the H^- ligand is observed in the EPR spectra of **19** and **20**, it is evident that the H^- ligand in both adducts occupies an equatorial position; axially bound hydride ($I = {}^1/_2$) in complexes with a d_{z^2} ground state is known to exhibit large proton hyperfine coupling.[35]

Structures and Reactivities of the Model Complexes: Similarities and Relevance to the Biological Nickel Site(s). The two DAPA complexes **8** and **9** contain TBP $[NiN_3E_2]$ (E = S, Se) chromophores. Recent XAS studies have shown that a TBP $[NiN_3S_2]$ core is a good mimic of the first coordination

(35) (a) Symons, M. C. R.; Aly, M. M.; West, D. X. *J. Chem. Soc., Chem. Commun.* **1979**, 51. (b) Morton, J. R.; Preston, K. F. *J. Chem. Phys.* **1984**, *81*, 5775.

Table 3. EPR Data DMF Glass, 100 K[a]

complex/enzyme	*g* (*A*, G)
$[Ni^I(terpy)(2,4,6\text{-}(Me)_3C_6H_2Se)_2(CO)]^-$ (**18**)	2.204, 2.131, 2.024 (12)
$[Ni^I(DAPA)(SPh)_2(CO)]^-$ (**12**)	2.198, 2.145, 2.023 (13)
$[Ni^I(DAPA)(SePh)_2(CO)]^-$ (**15**)	2.188, 2.145, 2.027 (13)
$[Ni^I(terpy)(2,4,6\text{-}(Me)_3C_6H_2Se)_2(H^-)]^{2-}$ (**21**)	2.240, 2.191, 2.047 (14.5)
$[Ni^I(DAPA)(SPh)_2(H^-)]^{2-}$ (**19**)	2.264, 2.220, 2.035 (14.5)
$[Ni^I(DAPA)(SePh)_2(H^-)]^{2-}$ (**20**)	2.262, 2.222, 2.036 (14.5)
T. roseopersicina[39]	2.19, 2.14, 2.01
Desulfovibrio gigas[1c]	2.19, 2.14, 2.02
Mb. thermoautotrophicum[1c]	2.196, 2.140, 2.000
D. baculatus ([FeNi]) (membrane-bound)[1c]	2.20, 2.16, 2.00
D. baculatus ([FeNiSe]) (periplasmic)[11b]	2.23, 2.17, 2.01
Desulfovibrio salexigens ([FeNiSe])[40]	2.22, 2.16, 2.02

[a] Spectrometer settings: microwave frequency, 9.43 GHz; microwave power, 13 mW; modulation frequency, 100 kHz; modulation amplitude, 2 G.

sphere of the nickel site in *T. roseopersicina* H_2ase.[10] The reactivities of these two model complexes, described in this account, clearly establish that the combined presence of aromatic heterocyclic nitrogens and thiolato sulfurs (or selenolato seleniums) in the first coordination sphere can provide stabilization to three oxidation states (+3, +2, and +1) of nickel in such chromophores. The proposed mechanism of the [FeNi] H_2ases that involves three oxidation states of nickel[2a,b,6,8] therefore seems to be a reasonable one.

The Ni-C signal of H_2ases arises from a key intermediate species formed during reductive activation of the enzymes under dihydrogen. At least three distinctly different formalisms have been suggested for this key intermediate. These three formalisms, namely, Ni(III)−H_2, Ni(III)−H^-, and Ni(I)−H^-, are largely speculative, and to date not one of these three possibilities has been confirmed unequivocally by chemical or spectroscopic means. It is important to note that the Ni-C signal appears under strictly reductive conditions, i.e., prolonged incubation under dihydrogen. Use of chemical oxidants 2,6-dichlorophenol−indophenol, $K_3Fe(CN)_6$) or exposure to dioxygen converts the C form of the enzyme back to the A/B form. It is therefore unlikely that the nickel center is in the +3 oxidation state in the C form.

The affinity of the biological nickel site toward CO also provides clues regarding the oxidation states of nickel in the different forms of the enzyme. CO does not bind to the oxidized forms (Ni-A/Ni-B) of the enzyme, where nickel is likely to be in the +3 oxidation state. The enzyme binds CO only in the C form, and such binding results in the loss of the Ni-C signal and the appearance of a new rhombic EPR signal of a CO adduct (referred to as the Ni-CO signal).[6a] The reactivities of the model complexes (**1**−**3**, **7**−**9**) also confirm that CO binds to the Ni(I) and not the Ni(III) species. Chemically, this is expected since CO is a very good π-acid ligand and binds to metals in low oxidation states. Taken together, results of the CO-binding studies with the enzymes as well as the model complexes support the presence of Ni(I) in the C forms of the H_2ases.

Since incubation of the CO-treated enzyme under dihydrogen restores the Ni-C signal,[6c] it is quite likely that the hydrogenic ligand is bound to a Ni(I) center in the C form of the enzyme. The most likely formalism for the Ni-C species is then Ni(I)−H^-. Indeed, with model complexes **2**, **3**, **7**−**9**, binding of H^- occurs only when the nickel centers are in the +1 oxidation state and the EPR parameters of the resultant hydride adducts are similar to those of the Ni-C signals of several H_2ases (Table 3 and ref 10a). This we believe is compelling evidence in favor of a Ni(I)−H^- formalism for the species responsible for the Ni-C signal. The absence of any proton hyperfine coupling and results of recent ENDOR studies on the Ni-C state of *D. gigas* H_2ase[34b] suggest the possibility of an in-plane hydride in such a species.[36] As discussed earlier, the H^- ligand in the hydride adducts of the reduced model complexes (like **19** and **20**) also resides in the equatorial plane.

That the model complexes **8** and **9** mimic the reactivity of the biological nickel site very closely is evidenced by their ability to react with dihydrogen at ambient temperature and pressure. When incubated under dihydrogen, **8** and **9** afford the Ni(I)−hydrides **19** and **20** in low yields. Clearly, H_2 acts as a reductant and the source of H^- in these reactions. Of great significance is the observation that the addition of a small amount of a base to solutions of **8** and **9** under dihydrogen increases the yields of the hydride adducts **19** and **20** to a considerable extent (Schemes 3 and 4). This increase is most likely due to a much higher concentration of H^- in the reaction mixtures containing the reduced (by H_2) model complexes. Heterolytic cleavage of H_2 (coordinated or not) in the presence of the base is the reason for this increase in the concentration of H^- in solution.[38]

The appearance of the Ni-C signal occurs only after long incubation of the enzymes under dihydrogen. This indicates that H_2 is not a strong reductant for the biological nickel site. This is also true for the model complexes. The extent of reduction by H_2 is small at ambient temperature and pressure. However, authentic Ni(I) species like **11** and **14** (formed with the aid of dithionite) react rapidly with H_2 in the presence of a base to afford very high yields of the Ni(I)−hydrides **19** and **20**. Heterolytic cleavage of H_2 in the vicinity of the Ni(I) centers therefore gives rise to the Ni(I)−hydrides as the final (and stable) product. We propose that a very similar sequence of reduction of the nickel center to Ni(I) followed by heterolytic cleavage of H_2 and formation of a stable Ni(I)−H^- intermediate is responsible for the appearance of the Ni-C signal. The possibility of a nearby basic residue serving as the proton acceptor during the heterolytic cleavage of dihydrogen at the enzymatic nickel site has been discussed in previous accounts.[7a] In the chemistry of the model complexes, NaOH (or other bases like thiolates) facilitates the crucial step of heterolytic cleavage of dihydrogen at or near the Ni(I) centers.

Summary and Conclusion

The following are the principal results and conclusions of this investigation.

(1) The distorted trigonal bipyramidal (TBP) complex [Ni(terpy)(2,4,6-$(Me)_3C_6H_2Se)_2$] (**7**) has been isolated from the

(36) Alternatively, the lack of hyperfine coupling in the Ni-C signal could be due to a H_2 molecule bound to the Ni center. However, this possibility would necessitate the presence of Ni(III) in the species responsible for the Ni-C signal. While a few metal−dihydrogen complexes have been reported recently,[37] these transition metal−H_2 complexes are extremely sensitive and readily bind N_2, CO, and CH_3CN molecules in place of H_2. In contrast, the Ni-C species as well as the hydride adducts of the reduced model complexes exhibit their characteristic EPR spectra in the presence of N_2, CO, and CN^- even at room temperature.

(37) (a) Kubas, G. J.; Ryan, R. R.; Swanson, B. I.; Vergamini, P. J.; Wasserman, H. J. *J. Am. Chem. Soc.* **1984**, *106*, 451. (b) Church, S. P.; Grevels, F. W.; Hermann, H.; Schaffner, K. *J. Chem. Soc., Chem. Commun.* **1985**, 30. (c) Morris, R. H.; Sawyer, J. F.; Shiralian, M.; Zubkowski, J. D. *J. Am. Chem. Soc.* **1985**, *107*, 5581.

(38) Since a small concentration of thiolate/selenolate is present in the solutions of the reduced model complexes **11** and **14** (due to partial loss of thiolate/selenolate in solution), the heterolytic cleavage of H_2 is possible with the aid of the free ligands (acting as base) even when no base is added. This is why the hydride adducts **19** and **20** form in low yields when H_2 is passed through solutions of **11** and **14** at room temperature (no base experiment).

(39) Cammack, R.; Bagyinka, C.; Kovacs, K. L. *Eur. J. Biochem.* **1989**, *182*, 357.

(40) Teixeira, M.; Moura, I.; Fauque, G.; Czechowski, M.; Berlier, Y.; Lespinat, P. A.; LeGall, J.; Xavier, A. V.; Moura, J. J. G. *Biochimie* **1986**, *68*, 75.

reaction of [Ni(terpy)Cl_2] and 2,4,6-$(Me)_3C_6H_2Se^-$ in acetonitrile. Reactions of [Ni(DAPA)Cl_2] with PhS^- and $PhSe^-$ in ethanol or acetonitrile also afford the distorted TBP complexes [Ni(DAPA)$(SPh)_2$] (**8**) and [Ni(DAPA)$(SePh)_2$] (**9**), respectively. The structures of **7**–**9** have been determined by X-ray crystallography. These three complexes add to the three previously reported TBP complexes, [Ni(terpy)$(C_6F_5S)_2$] (**1**),[10b] [Ni(terpy)-(2,4,6-(*i*-Pr)$_3C_6H_2S)_2$] (**2**),[10b] and [Ni(terpy)$(2,6\text{-}(Me)_2C_6H_3S)_2$] (**3**),[10a] that contain the $[NiN_3E_2]$ (E = S, Se) chromophore and serve as good structural models of the nickel site in *T. roseopersicina* H_2ase.

(2) With the more compact terpy ligand as the 3N donor, coordinatively unsaturated yet monomeric Ni(II) complexes **1**–**3** and **7** are isolated only with aryl thiolates and selenolates with bulky substituents. Free rotation of the phenyl groups of the 3N donor DAPA ligand, on the other hand, covers more space around the nickel center, thus allowing isolation of the pentacoordinated Ni(II) complexes **8** and **9** with simple PhS^- and $PhSe^-$. Monomeric Ni(II) complexes with one open coordination site could therefore be synthesized by introducing steric hindrance through either the 3N donor ligand or the thiolates/selenolates.

(3) Upon reduction with aqueous dithionite, the terpy analogues (**1**–**3**, **7**) afford the corresponding Ni(I) species that bind CO (reversibly) and H^-. The EPR parameters of these CO and hydride adducts resemble the Ni-CO and Ni-C signals of the H_2ases. Oxidation of the terpy analogues with common oxidants, however, proceeds to a marginal extent and gives rise to unstable Ni(III) species.

(4) The two DAPA complexes **8** and **9** belong to the first set of analogues with the desired $[NiN_3E_2]$ (E = S, Se) chromophore that undergoes facile oxidation and reduction with biologically relevant oxidants and reductants to afford the corresponding Ni(III) and Ni(I) species. The transformation Ni(III) ← Ni (II) → Ni(I) is reversible. Attainment of three oxidation states of nickel in a structural mimic of the biological nickel site, an important characteristic of a functional model, has therefore been achieved in **8** and **9**.

(5) Oxidation of the DAPA complexes **8** and **9** with $[Fe(CN)_6]^{3-}$ gives rise to the Ni(III) species **10** and **13** in significant yields. Both **10** and **13** exhibit EPR spectra with the single electron in the d_{z^2} orbital and do *not* bind CO. The S-containing species **10** is comparatively more stable.

(6) Reduction of **8** and **9** by aqueous dithionite readily affords the Ni(I) species **11** and **14**. The single electron in these Ni(I) complexes resides in the $d_{x^2-y^2}$ orbital. Both **11** and **14** bind CO reversibly, much like the enzyme. The affinity of the reduced (Ni(I)) nickel centers in **11** and **14** toward CO strongly suggests that the biological nickel center in the C form exists in the +1 oxidation state (H_2ases bind CO only in the Ni-C forms). Upon standing at room temperature, **11** and **14** lose thiolate/selenolate ligands to produce $[Ni^I(DAPA)(solv)_2]^+$ (**16**). The loss of thiolate ligands from **11** is a much faster process. Though **16** by itself does not bind CO, it does so in the presence of 2 equiv of thiolate/selenolate ligand. Clearly, binding of CO (a strong π-acceptor) at the Ni(I) centers in **11** and **14** is facilitated by the presence of the thiolate/selenolate ligands (good electron donors).

(7) Reaction of **8** and **9** with $NaBH_4$ at low temperatures produces the Ni(I) hydride adducts **19** and **20**. The presence of a small (~0.2 equiv) amount of a base like NaOH improves the yields of the hydride adducts in such reactions. When **19** and **20** are synthesized from the Ni(I) species **11** and **14** (generated independently by aqueous dithionite) and 0.5 equiv of $NaBH_4$, the presence of a base in the reaction mixture is essential. Clearly, the hydride adducts are more stable under basic conditions. The EPR features of the rhombic EPR spectra of **19** and **20** resemble those of the Ni-C signals of the H_2ases (Table 3). This similarity supports the Ni(I)–H^- formalism for the nickel site in form C of the H_2ases. The absence of detectable proton hyperfine coupling in the EPR spectra of the model complexes as well as the enzymes indicates that the bound hydride ligand resides at the equatorial plane.

(8) In DMF solutions containing small amounts of a base like NaOH, the two DAPA complexes **8** and **9** react with dihydrogen to produce the Ni(I) hydride adducts **19** and **20**. Authentic Ni(I) species like **11** and **14** react more readily with dihydrogen in the presence of a base to give **19** and **20** in significant yields. This reactivity toward dihydrogen at ambient temperature and pressure is especially notable since the model complexes mimic the reductive activation step of the biological nickel site in such a reaction to ultimately produce Ni-C-like EPR signals. In addition, the observed enhancement of the intensities of the EPR signals of the hydride adducts in the presence of a base indicates heterolytic cleavage of H_2 (coordinated or not) at the Ni(I) site. A similar chemistry at the enzyme active site is proposed.

At the present time, research in this laboratory has been directed toward isolation and further characterization of the various Ni(I) CO and hydride adducts. Additional experiments are in progress to establish the conditions for catalytic hydrogen evolution by the DAPA complexes. The results will be reported elsewhere.

Acknowledgment. Financial support from the donors of the Petroleum Research Fund, administered by the American Chemical Society, is gratefully acknowledged.

Supplementary Material Available: EPR spectra showing stepwise oxidation of **12** with $[Fe(CN)_6]^{3-}$ and loss of coordinated CO during the oxidation process (Figure S1) and crystal structure data for **7**–**9** including atomic coordinates and isotropic thermal parameters for the non-hydrogen atoms (Tables S1–S3), complete lists of bond distances (Tables S4–S6) and angles (Tables S7–S9), anisotropic thermal parameters (Tables S10–S12), and H atom coordinates (Tables S13–S15) (30 pages); values of $10|F_o|$ and $10|F_c|$ (Tables S16–S18), (80 pages). This material is contained in many libraries on microfiche, immediately follows this article in the microfilm version of the journal, and can be ordered from the ACS; see any current masthead page for ordering information.

JA941172X